Electronic Supplementary Information (ESI)

A Mixed Ion-Electron Conducting Network Derived from Porous CoP Film for Stable Lithium Metal Anodes

Xin Cao[a] †, Qian Wang[b] †, Hangchao Wang[a], Zhicheng Shang[a], Jinli Qin[a], Wen Liu[a] *, Henghui Zhou[b] and Xiaoming Sun[a]

a College of Chemistry, State Key Laboratory of Chemical Resource Engineering, Beijing Advanced Innovation Center for Soft Matter Science and Engineering, Beijing University of Chemical Technology, Beijing 100029, China

b College of Chemistry and Molecular Engineering, Peking University, Beijing 100871, China

E-mail: wenliu@mail.buct.edu.cn

† These authors contributed equally to this work.

Note 1: Tafel plot and calculation of the exchange current density (i^0)

Tafel plot can be obtained by fitting Tafel equation in the overpotential region with kinetic control (-0.05 to 0.05 V *vs* Li^+/Li in our case):

$$\eta = -\frac{2.3RT}{\alpha nF} lgi^0 + \frac{2.3RT}{\alpha nF} lgi$$

Where η is the overpotential for Li plating/stripping and i is the corresponding current densit, α is the energy transfer coefficient, and i^0 is the exchange current density. Fitting the larger overpotential area in the Tafel curve to a straight line, the slope of the straight line is 2.3RT/αnF, and the intercept of the straight line at η equal to 0 is lgi^0.

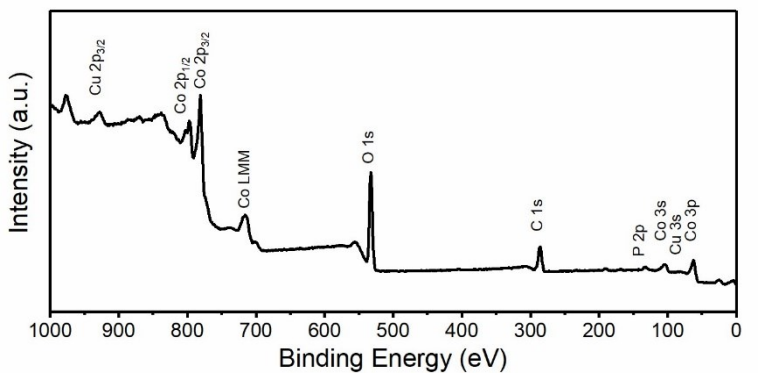

Figure S1. XPS spectrum of the porous CoP film prepared by electrochemical deposition.

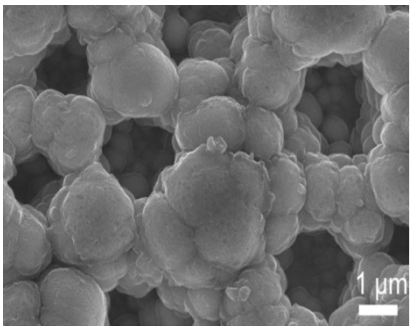

Figure S2. SEM image of the porous CoP film electrode after lithiation, which can still maintain its porous structure

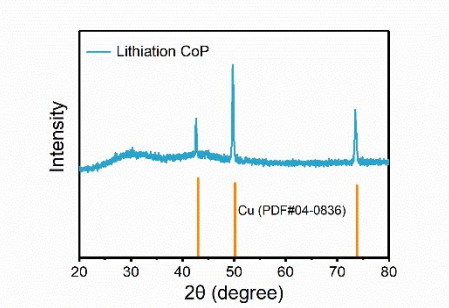

Figure S3. XRD pattern of the porous CoP film after lithiation, which only shows the diffraction peaks of Cu substrate, demonstrating the amorphous feature of the lithiation products.

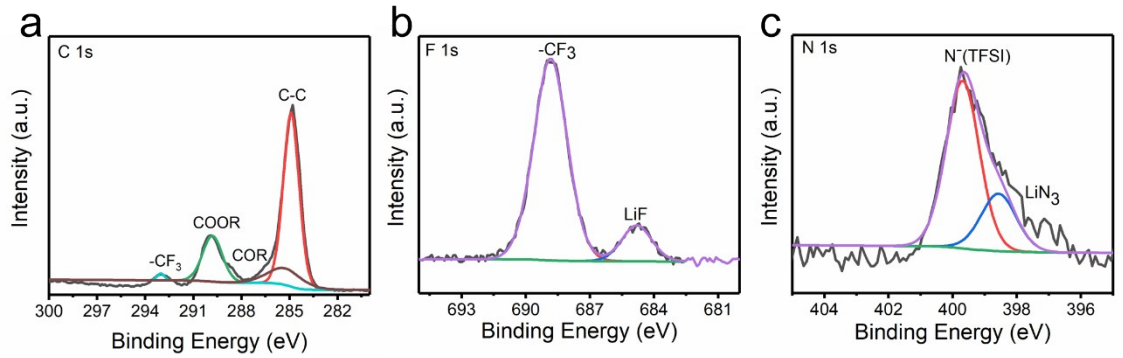

Figure S4. XPS spectra of the porous CoP film electrode after lithiation. (a) C 1s, (b) F 1s, and (c) N 1s.

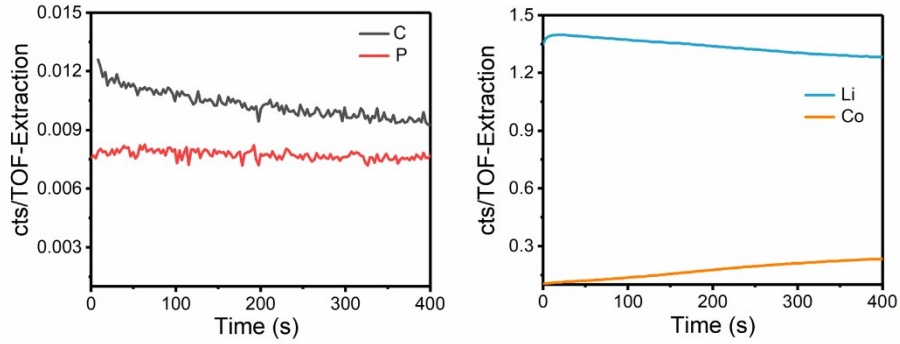

Figure S5. TOF-SIMS depth profiles of the C, Li, Co, and P species in the porous CoP film electrodes after discharge to 0.01 V (lithiation).

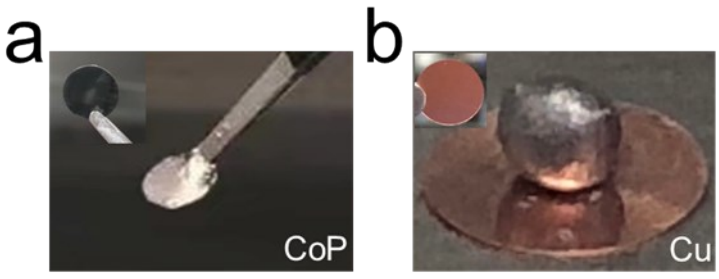

Figure S6. Surface wetting of molten Li on (a) porous CoP film (b) Planer Cu.

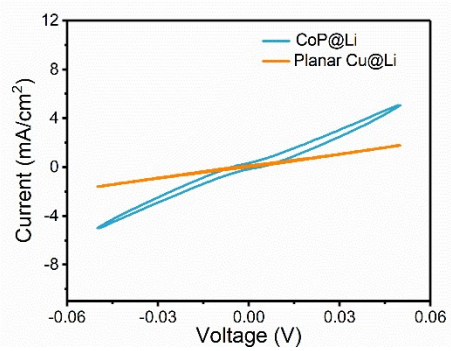

Figure S7. The CV curves of planar Cu@Li and CoP@Li anode.

Figure S8. Photograph of the battery undergoing in-situ Li plating measurement.

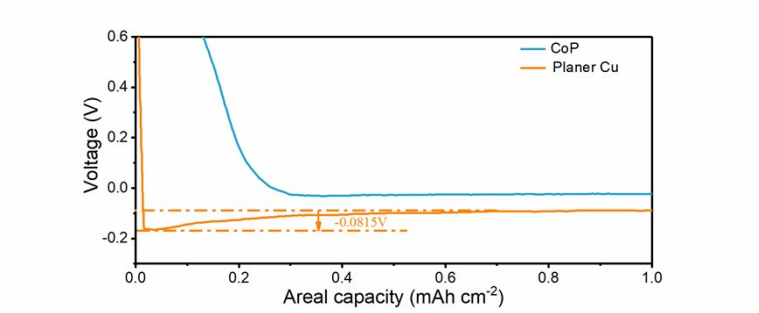

Figure S9. Voltage-capacity curves of planar Cu and porous CoP film electrode at current density of 1 mA cm^{-2} during the first cycle.

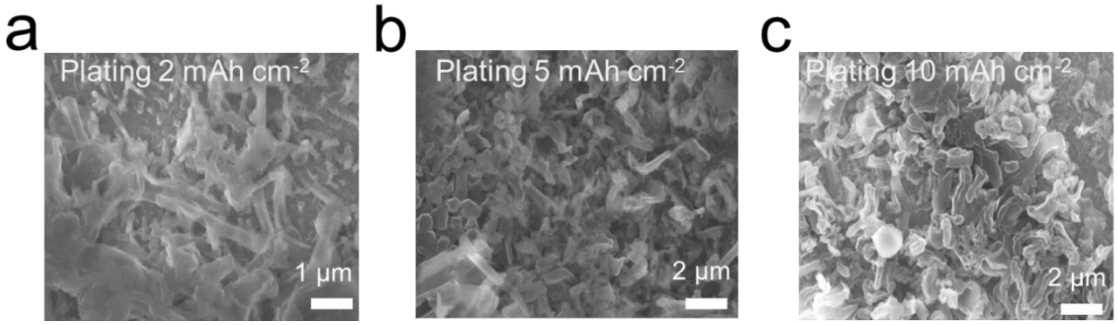

Figure S10. SEM images of Li metal deposited on planer Cu electrode at a current density of 1 mA cm^{-2} with different capacity. (a) 2 mAh cm^{-2}, (b) 5 mAh cm^{-2}, (c) 10 mAh cm^{-2}

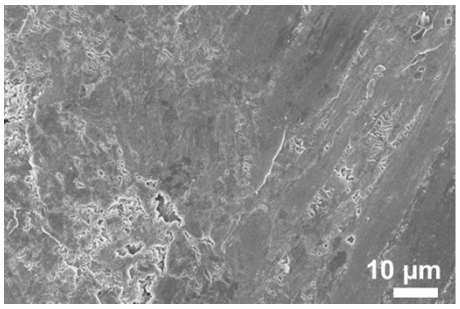

Figure S11. SEM image of lithium deposition in the porous CoP host after 50 cycles at the current density of 1 mA cm^{-2} and the capacity of 10 mAh cm^{-2}.

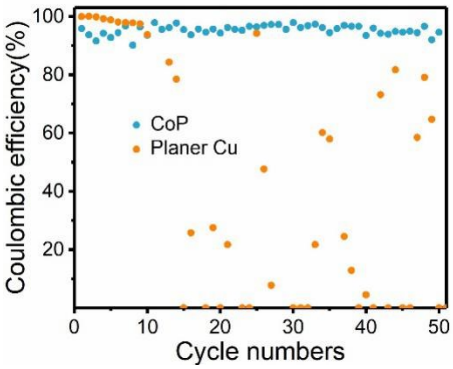

Figure S12. Coulombic efficiencies of Li||Cu half cells using planar Cu and porous CoP film as working electrodes with deposition capacity and current density of 5 mA cm^{-2} and 1 mAh cm^{-2}

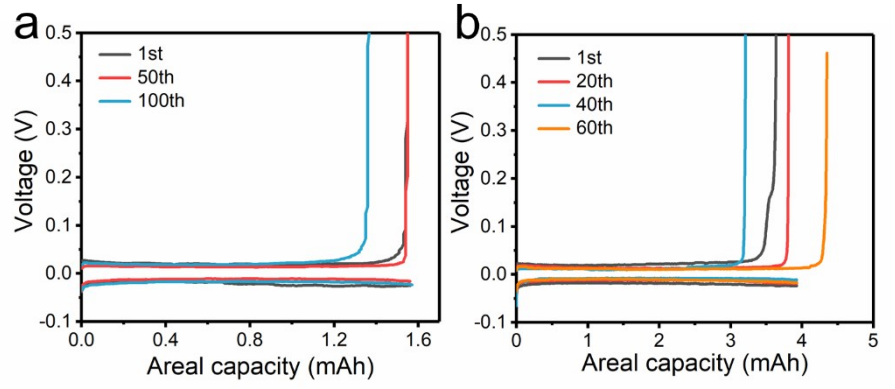

Figure S13. Voltage profiles of the planer Cu electrode with the deposition capacity and current density of: (a) 2 mAh cm^{-2} and 1 mA cm^{-2}, (b) 5 mAh cm^{-2} and 1 mA cm^{-2}.

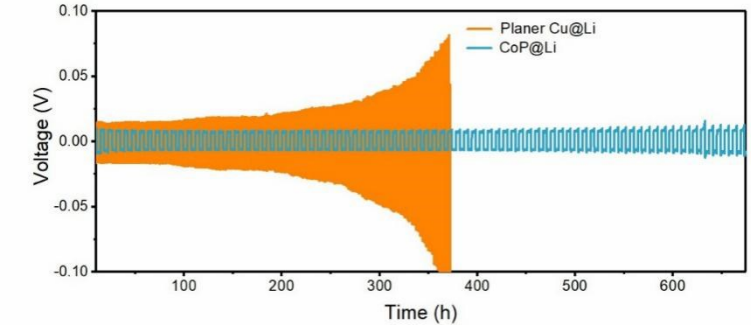

Figure S14. Cycling performance of the symmetric cells with fixed capacity of 2 mAh cm^{-2} at the current density of 0.5 mA cm^{-2} of CoP@Li and Cu@Li.

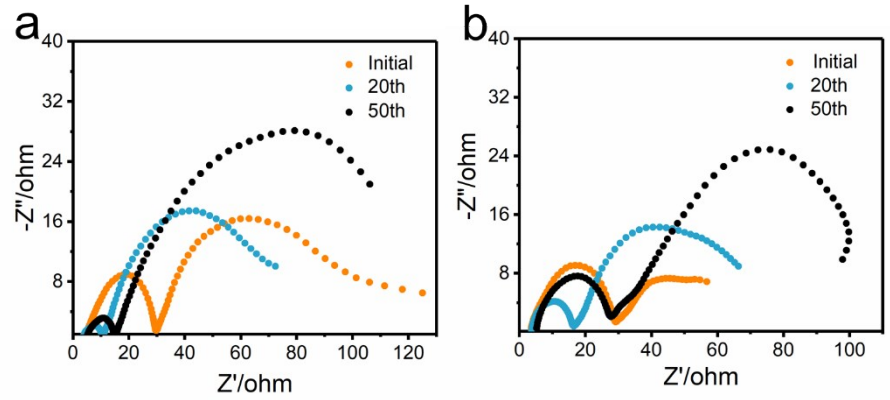

Figure S15. EIS plots of Li||Li symmetric cells before and after different cycles with the current density of 1 mA cm^{-2} and the capacity of 1 mAh cm^{-2}. (a) EIS plots for the CoP@Li||CoP@Li symmetric cells; (b) EIS plots for the planar Cu@Li||planer Cu@Li symmetric cells.

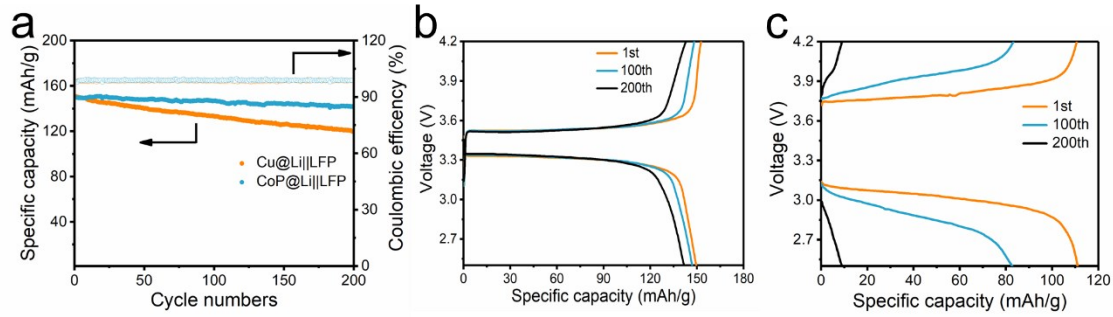

Figure S16. Cycling performance of Li metal full cells. (a) The discharge capacity and coulombic efficiency *vs*. cycle numbers of CoP@Li||LFP and Cu@Li||LFP. (b) Voltage profiles of CoP@Li|LFP cell at 1 C after different cycles. (c) Voltage profles of the Cu@Li||LFP cell at 5 C after different cycles.

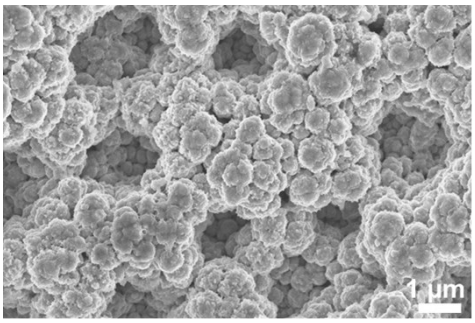

Figure S17. SEM images of porous CoP framework after 200 cycles at 1 C in the CoP@Li||LFP cell.

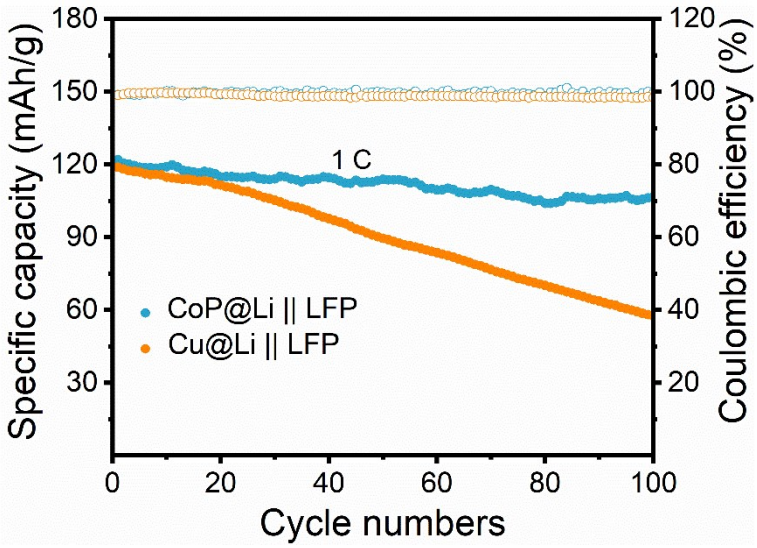

Figure S18. Cycling performance of CoP@Li||LFP and Cu@Li||LFP with a low N/P ratio of 1.5 at 1 C.

Table S1: Comparison of half-cell electrochemical performance.

Scaffold	Capacity/mAh cm^{-2} and Current/mA cm^{-2}	Cycle numbers	Coulombic efficiency	References
Cu_3N nanoparticles incorporating styrene butadiene rubber[1]	1, 1	100	97.4%	*Adv Mater*
3D porous Cu current collector[2]	1, 0.5	50	97%	*Nat Commun*
Graphitized carbon fibers[3]	1, 1	50	98%	*Adv Mater*
CuO Nanosheets[4]	1, 0.5	180	94%	*Advanced Energy Materials*
3D Cu@Al host[5]	2, 0.5	85	98.6%	*Angew Chem*
g-C_3N_4@Ni foam[6]	1, 0.5	300	98%	*Advanced Energy Materials*
Nanofiber graphene Aerogel host[7]	3, 1	100	98.5%	*Small*
Crumpled graphene balls[8]	1, 1	50	94%	*Joule*
3D glass fiber cloths[9]	0.5, 1	65	97%	*Adv Mater*
3D gold-modified Ni foam[10]	1, 0.5	100	98%	*Energy Storage Mater*
3D conductivity and lithiophilicity gradients host[11]	2, 0.5	350	97%	*Nat Commun*
This work	2,1	250	98.63%	
	5,1	80	98.4%	
	10,1	50	97.92%	
	1,5	50	95.4%	

References:

1 Y. Liu, D. Lin, P. Y. Yuen, K. Liu, J. Xie, R. H. Dauskardt, et al., An Artificial Solid Electrolyte Interphase with High Li-Ion Conductivity, Mechanical Strength, and Flexibility for Stable Lithium Metal Anodes, *Adv Mater*, 2017, **29**, 1605531 ;

2 C. P. Yang, Y. X. Yin, S. F. Zhang, N. W. Li and Y. G. Guo, Accommodating lithium into 3D current collectors with a submicron skeleton towards long-life lithium metal anodes, *Nat Commun*, 2015, **6**, 8058;

3 S. H. Wang, Y. X. Yin, T. T. Zuo, W. Dong, J. Y. Li, J. L. Shi, et al., Stable Li Metal Anodes via Regulating Lithium Plating/Stripping in Vertically Aligned Microchannels, *Adv Mater*, 2017, **29**, 1703729 ;

4 C. Zhang, W. Lv, G. Zhou, Z. Huang, Y. Zhang, R. Lyu, et al., Vertically Aligned Lithiophilic CuO Nanosheets on a Cu Collector to Stabilize Lithium Deposition for Lithium Metal Batteries, *Advanced Energy Materials*, 2018, **8**, 1703404 ;

5 H. Ye, Z. J. Zheng, H. R. Yao, S. C. Liu, T. T. Zuo, X. W. Wu, et al., Guiding Uniform Li Plating/Stripping through Lithium-Aluminum Alloying Medium for Long-Life Li Metal Batteries, *Angew Chem Int Ed Engl*, 2019, **58**, 1094-1099;

6 Z. Lu, Q. Liang, B. Wang, Y. Tao, Y. Zhao, W. Lv, et al., Graphitic Carbon Nitride Induced Micro-Electric Field for Dendrite-Free Lithium Metal Anodes, *Advanced Energy Materials*, 2019, **9**, 1803186;

7 C. Zhao, C. Yu, S. Li, W. Guo, Y. Zhao, Q. Dong, et al., Ultrahigh-Capacity and Long-Life Lithium-Metal Batteries Enabled by Engineering Carbon Nanofiber-Stabilized Graphene Aerogel Film Host, *Small*, 2018, **14**, e1803310;

8 S. Liu, A. Wang, Q. Li, J. Wu, K. Chiou, J. Huang, et al., Crumpled Graphene Balls Stabilized Dendrite-free Lithium Metal Anodes, *Joule*, 2018, **2**, 184-193;

9 X. B. Cheng, T. Z. Hou, R. Zhang, H. J. Peng, C. Z. Zhao, J. Q. Huang, et al., Dendrite-Free Lithium Deposition Induced by Uniformly Distributed Lithium Ions for Efficient Lithium Metal Batteries, *Adv Mater*, 2016, **28**, 2888-2895;

10 X. Ke, Y. Liang, L. Ou, H. Liu, Y. Chen, W. Wu, et al., Surface engineering of commercial Ni foams for stable Li metal anodes, *Energy Storage Materials*, 2019, **23**, 547-555;

11 J. Pu, J. Li, K. Zhang, T. Zhang, C. Li, H. Ma, et al., Conductivity and lithiophilicity gradients guide lithium deposition to mitigate short circuits, *Nat Commun*, 2019, **10**, 1896;